
On using a Lagrangian model to calibrate primary production determined from *in vitro* incubation measurements

W. Barkmann and J.D. Woods¹

Southampton Oceanography Centre, Oceanography Department, Southampton SO14 3ZH and ¹Earth Resources Engineering Department, Imperial College, London, UK

Abstract. This paper discusses an observing system simulation experiment which reveals the difference in primary production of (i) phytoplankton moving freely in the turbulent mixed layer of the upper ocean and (ii) a sample of the same population held in a bottle at fixed depths. The results indicate the tendency of incubation measurements to overestimate phytoplankton production rates by up to 40%. Differences in primary production depend to a first approximation on the vertical extent of mixing and on water turbidity. A simple model was constructed leading to a non-linear calibration function which relates the difference in primary production to surface irradiance, mixing depth and to the depth of the euphotic zone. This function has been applied to calibrate the production rates simulated at fixed depths, and the corrected values were verified by comparisons with productivities in the turbulent environment. The calibration function was found to be capable of reducing the differences significantly.

Introduction

A widely used method of measuring primary production in the sea is the ¹⁴C *in vitro* incubation method. In this method, water samples are chosen from different depths, small amounts of a radioactive bicarbonate are added, and the sample bottles are suspended in the ocean between dawn and dusk. The daily primary production is calculated from the amount of radioactive carbon assimilated by the plankton cells held in the bottles during the incubation period. This method does not take into consideration physiological responses due to changes in the ambient light in a turbulence environment, and therefore may be capable of measuring precise production rates in the upper ocean only if turbulent mixing is negligible. However, the upper ocean boundary layer in general is in a state of permanent turbulence, and plankton cells are forced up and down a vertical irradiance gradient during daylight. Observations show that turbulence profiles comprise a surface layer with continuous power supply of order mW m^{-2} , bounded by a sharp turbocline, below which the turbulence occurs intermittently with a mean power supply of order $\mu\text{W m}^{-2}$. The depth of the turbocline had been observed to exhibit diurnal excursions over many tens of metres (Woods, 1968).

Phytoplankton trapped in the turbulence environment experience strong fluctuations in solar irradiance, and the vertical gradients of photoadaptive properties of plankton may change according to the environmental stress conditions (Lewis *et al.*, 1984). In the past, a number of field and laboratory experiments have been performed to study the response of physiological parameters and phytoplankton growth to fluctuating light (Marra, 1978a,b; Gallegos and Platt, 1982; Yoder and Bishop, 1985). In general, these studies were restricted to specific environmental conditions like constant and shallow mixed layers and weak mixing, and the turbulence environment was simulated by fluctuating light or by sample bottles cycled

between the surface and a fixed depth. The numerical experiments of Lande and Lewis (1989) and Falkowski and Wirick (1981) are based on similar environmental restrictions.

Here, we report the results of a numerical simulation which includes a more comprehensive spectrum of environmental fluctuations, e.g. water turbidity is related to plankton biomass profile, and changes in the mixing depth are controlled by seasonal and diurnal astronomical cycles as well as by synoptic scale wind fluctuations. Photoadaptive variables follow the rules of the diatom *Thalassiosira pseudonana* as specified by Cullen and Lewis (1988). The study comprises integrations at different locations in the North Atlantic during the spring bloom.

The ecology model

We used the Woods and Barkmann (1994) one-dimensional ecology model comprising (i) a phytoplankton model based on a quota method for growth and reproduction (internal carbon and nitrogen pools), (ii) a model of vertical migration and growth of herbivorous zooplankton and (iii) a physical upper ocean boundary-layer model forced by surface buoyancy and momentum fluxes.

The biological model is integrated by using the Lagrangian ensemble method; this approach explicitly represents ensembles of several thousand particles each carrying a changing load of cells and moving through the water column like individual plankters. The minimum requirement for the model is to keep 20 particles per 1 m depth interval in the mixing layer, since test studies have shown that a higher number of particles did not change the results significantly.

The physical environment is controlled by fluxes through the sea surface by means of (i) a Kraus–Turner (1967) type mixed-layer model (Woods and Barkmann, 1986) designed to simulate accurately the response of turbocline depth to diurnal and seasonal changes in surface heat flux as well as to varying wind stress, and by (ii) a random walk model to simulate particle motion in the turbulent boundary layer.

Photosynthesis and nutrient uptake

The model equations for photosynthesis applied in this study differ from those described in Woods and Barkmann (1993) who used a single exponential parameterization based on Steele (1962). Here, we use the PI curve of Platt *et al.* (1980) to parameterize photosynthetic processes.

The increase of the internal carbon pool C_p in each phytoplankton cell is given by:

$$\frac{1}{C} \frac{\partial C_p}{\partial t} = \theta^{-1} P_m (1 - e^{-\frac{\alpha I}{P_m}}) e^{-\frac{\beta I}{P_m}} - R_p \quad (1)$$

where C represents the carbon content of a cell, I is the ambient irradiance at particle depth and R_p is the CO_2 loss due to respiration.

The photoadaptive variables θ , α , P_m , β represent the carbon–chlorophyll ratio, the initial slope of the PI curve, photosynthesis at light saturation and a parameter which takes into account the effect of photoinhibition.

Table I. Cells-specific constants of *T.pseudonana* [from Lande and Lewis (1989) and Cullen and Lewis (1988)]

	γ (h ⁻¹)	b	a
α [$\mu\text{g C } \mu\text{g}^{-1} \text{ Chl } (\mu\text{E m}^{-2} \text{ s}^{-1})^{-1}$]	0.58	0.0527	-0.00468
β [$\mu\text{g C } \mu\text{g}^{-1} \text{ Chl } (\mu\text{E m}^{-2} \text{ s}^{-1})^{-1}$]	0.50	0.00438	-0.000733
P_m [$\mu\text{g C } \mu\text{g}^{-1} \text{ Chl h}^{-1}$]	0.29	-0.86	0.968
θ [$\mu\text{g C } \mu\text{g}^{-1} \text{ Chl}$]	0.14	-34.7	15.77

In order to address photosynthesis in a changing light environment, we adapted the approach taken by Lande and Lewis (1989) by using a logarithmic light dependence of the variables, and first-order kinetics to simulate the effect of photoadaptation.

$$\alpha^* = b_\alpha + a_\alpha \ln(I), \quad \beta^* = b_\beta + a_\beta \ln(I) \quad (2)$$

$$P_m^* = b_{P_m} + a_{P_m} \ln(I), \quad \theta^* = b_\theta + a_\theta \ln(I)$$

$$\frac{d\alpha}{dt} = \gamma_\alpha(\alpha^* - \alpha), \quad \frac{d\beta}{dt} = \gamma_\beta(\beta^* - \beta) \quad (3)$$

$$\frac{dP_m}{dt} = \gamma_{P_m}(P_m^* - P_m), \quad \frac{d\theta}{dt} = \gamma_\theta(\theta^* - \theta)$$

where $(\gamma_{\theta, \alpha, \beta, P_m})^{-1}$ are the time scales of photoadaptation for each of the three parameters.

$\theta, \alpha, \beta, P_m$ represent the photoadaptive variables, and $\theta^*, \alpha^*, \beta^*, P_m^*$ are the values towards which they are physiologically adapting; $b_{\theta, \alpha, \beta, P_m}, a_{\theta, \alpha, \beta, P_m}, \gamma_{\theta, \alpha, \beta, P_m}$ are cell-specific constants which are presented in Table I. We follow Falkowski and Wirick (1986), who stated that plankton cells do not adapt at night by setting $\gamma_{\theta, \alpha, \beta, P_m}$ equal to zero between sunset and sunrise.

Useful variables are I_k and I_{opt} , where I_k is defined as P_m/α (the light range in which photosynthesis is approximately a linear function of light) and I_{opt} is the irradiance at which photosynthesis has its maximum.

For the uptake of nitrate $N(z)$ and ammonium $A(z)$, the Michaelis-Menten kinetics are used, with equal preference for nitrate and ammonium.

$$\frac{\partial N_p}{\partial t} = \frac{\frac{N(z)}{k_n} + \frac{A(z)}{k_a}}{1 + \frac{N(z)}{k_n} + \frac{A(z)}{k_a}}$$

Cell division takes place when both the carbon and the nitrogen pool exceed a prescribed threshold value (which is determined by the volume of a plankton cell).

The coupled model is forced by a stochastic wind superimposed on climatological surface momentum and turbulent buoyancy fluxes, and by a diurnally vary-

ing solar radiation and climatological cloud cover. Integrations have been carried out at two different locations, i.e. 55°N 37°W and 41°N 27°W.

Particle motion in a turbulent boundary layer

Random walk models of particle motions have long been used to estimate dispersion of particles in turbulent air (e.g. Hall, 1975; de Baas *et al.*, 1986; Thomson, 1986), and they have been applied to the upper ocean boundary layer, to simulate vertical motions of phytoplankton particles in Lagrangian models (Falkowski and Wirick, 1981; Lande and Lewis, 1989; Yamazaki and Kamykowski, 1991). In the latter approach, the Lagrangian properties of the particles were related to vertical diffusion coefficients. In this study, velocity variance and Lagrangian time scale are estimated from the turbulent kinetic energy (TKE) budget of a bulk mixed-layer model assuming homogeneous and isotropic turbulence.

The dispersion of plankton cells in a homogeneous turbulent boundary layer is simulated by the classical Langevin equation:

$$dV = \frac{V}{\tau} dt + d\zeta \tag{4}$$

where V is the velocity of a particle, τ the Lagrangian time scale and $d\zeta$ a random velocity increment. Particles are reflected at both the sea surface and the mixed-layer base.

In homogeneous turbulence, $d\zeta$ may be described by:

$$\overline{(d\zeta)} = 0, \quad \overline{(d\zeta)^2} = \frac{2\overline{u^2}}{\tau} dt, \quad \overline{(d\zeta)^3} = 0$$

where $\overline{u^2}$ is the variance of the turbulent velocity.

The variance of the two unknown parameters in equation (4) (τ and $\overline{u^2}$) may be estimated from the TKE budget of the simulated turbulent boundary layer. The variance is consistent with the velocity scale simulated by the mixed-layer model.

The vertically integrated and parameterized equations of the TKE budget in a bulk mixed layer can be written as:

$$m_1 u_*^3 + m_2 u_*^3 = \int_{-h}^0 b' w' dz + h \epsilon_m$$

(I) (II) (III) (IV)

(I) and (II) are production terms of TKE due to breaking surface waves and current shear instabilities, respectively. (III) is a source or sink of TKE either due to convection or entrainment, and (IV) presents the vertically integrated dissipation rate.

Assuming isotropic turbulence ($\overline{u_1^2} = \overline{u_2^2} = \overline{u_3^2}$), the mean TKE E can be written as:

$$E = \frac{1}{2} (\overline{u_1^2} + \overline{u_2^2} + \overline{u_3^2}) = \frac{3}{2} \overline{u^2}$$

In order to estimate the TKE from the existing mixed-layer model, Kolmogorov's parameterization of TKE dissipation is applied:

$$h\epsilon_m = \frac{hE^{3/2}}{l_t}$$

where

$$h\epsilon_m = mu^3(1 - e^{-h/\lambda}) + (1 - n)P_c$$

P_c is a TKE source due to convection and is calculated from a convection depth (Woods and Barkmann, 1986). $m = m_1 + m_2 = 0.8$, $n = 0.1$ and $\lambda = 100 \text{ m}$ are model parameters, h is the depth of the turbulent boundary layer and u_* the friction velocity in water. The variance of the turbulent velocity is then given by:

$$\overline{u^2} = \frac{2}{3} \left[\frac{l_t}{h} (mu^3(1 - e^{-h/\lambda}) + (1 - n)P_c) \right]^{2/3}$$

In homogeneous isotropic turbulence, the Lagrangian time scale may be approximated by:

$$\tau = a^{-1} l_t (\overline{u^2})^{-1/2}$$

l_t is a dissipation length which is linked to the size of the most energetic eddies and a is a parameter of order 3 (Tennekes and Lumley, 1972). In this study, the dissipation length l_t was chosen to be represented by the mixing layer depth, h .

A time step of 6 min was used, which resolves the Lagrangian time scales calculated from the model.

Surface buoyancy and momentum fluxes

In order to simulate various mixed-layer depth fluctuations, the mixed-layer model was forced by a stochastic wind (u') superimposed on monthly mean values (\bar{u}) (Isemer and Hasse, 1987). The wind energy spectrum in subseasonal scales of the North Atlantic Ocean is calculated from a Gaussian energy distribution with a maximum at a period of 6 days (synoptic peak) (Byshev and Ivanov, 1969). The corresponding turbulent surface buoyancy flux, b , was approximated by

$$b = \bar{b} \left(1 + \frac{u'}{\bar{u}} \right), \text{ where } \bar{b} \text{ is the climatological monthly mean value.}$$

To resolve the diurnal cycle of the boundary layer, the surface short-wave radiation is calculated using a radiation model based on Paltridge and Platt's (1976) empirical parameterizations of the atmospheric transmission of solar radiation (Horch *et al.*, 1983). The vertical distribution of solar irradiance inside the ocean is determined by employing the attenuation coefficients for downwelling radiation in pure water from Woods (1980) in the 300–2500 nm waveband, and the chlorophyll specific attenuation coefficients for wavelengths between 400 and 700 nm from Morel (1988).

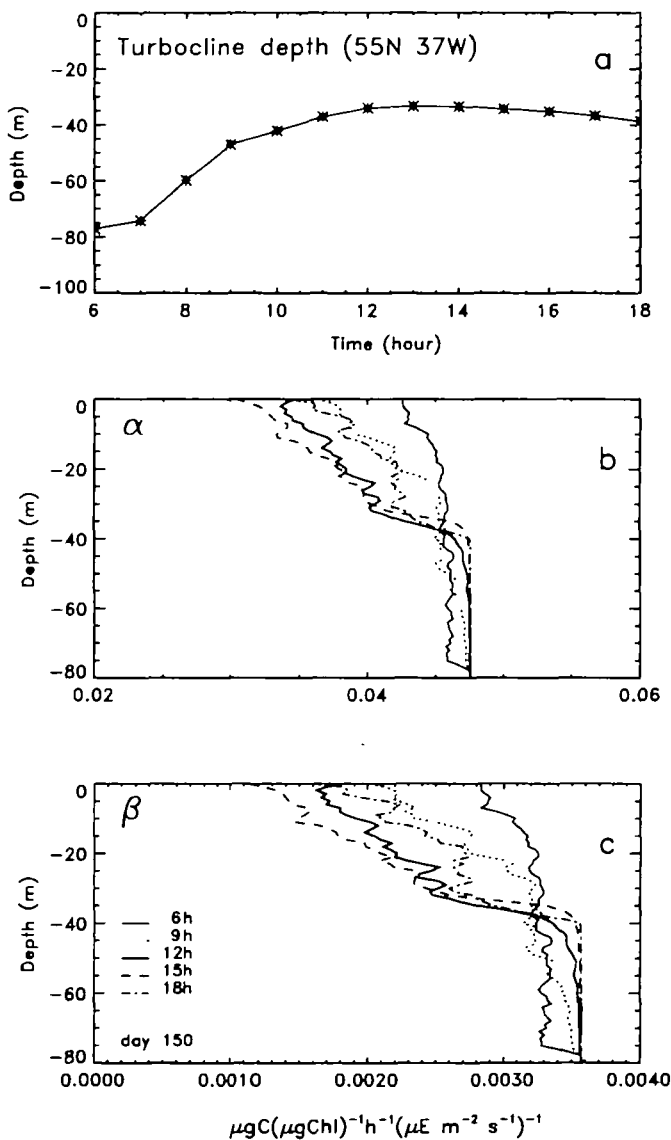


Fig. 1. (a-c) Depth of the mixing layer and profiles of the photoadaptive parameters α and β in the mixed water column at day 150.

Results

Profiles of photosynthesis and photoadaptive variables

The model was integrated over a time period of 140 days starting on 2 March (day 61), and the model results for 30 May (day 150) were chosen to discuss characteristic diurnal cycles of photosynthesis and the related variables. The photoadaptive variables and the photosynthetic rates presented here are averaged values (averaged over all cells contained in a 1 m depth interval).

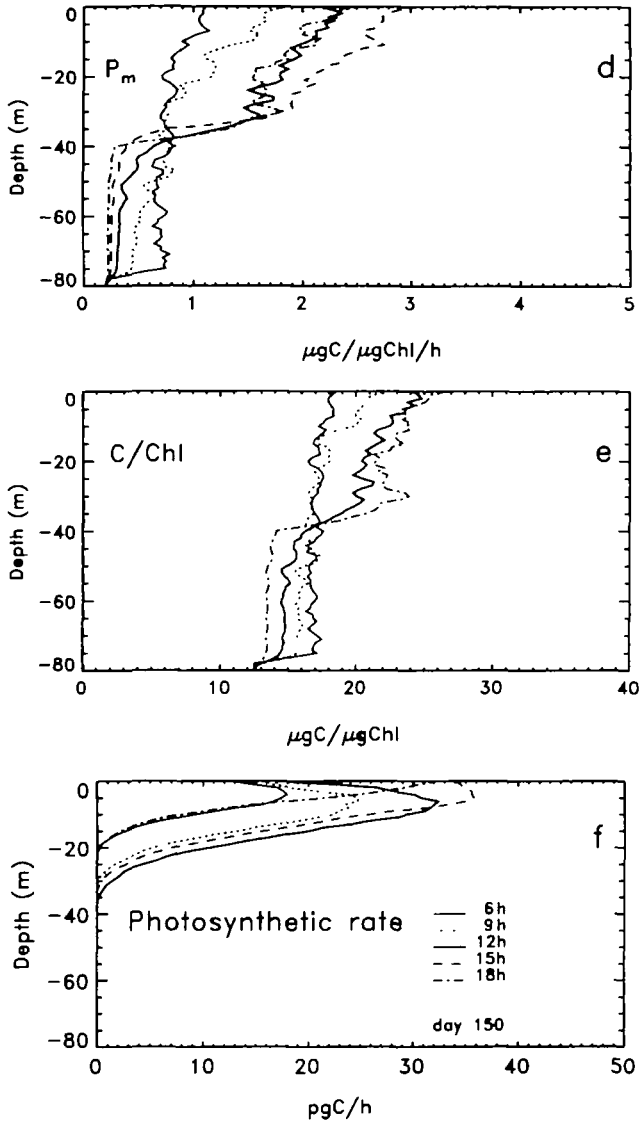


Fig. 1. (d–f) Profiles of the photoadaptive parameters θ and P_m and of photosynthesis in the mixed water column at day 150.

Typical profiles of the photoadaptive variables between sunrise and sunset are shown in Figure 1b–e. The profiles are characterized by a strong vertical gradient at the base of the turbulent layer in the afternoon, a weak gradient within the mixing layer and a quasi-constant value in the diurnal thermocline. The diurnal changes are asymmetrical. Maximum (minimum) values can be found in the afternoon, with a slight decrease (increase) between 12.00 and 15.00 h.

The diurnal variations of the photoadaptive variables have a significant effect on the photosynthesis of phytoplankton cells. Maximum photosynthesis occurs in the afternoon between 12.00 and 15.00 h in the upper 10 m (Figure 1f). During the morning hours, photoinhibition can become important in the near-surface layers because β is still high.

The asymmetry of the photosynthetic rates between morning and afternoon is mainly a consequence of photoadaptation. During the morning hours, the ambient irradiance is much higher than the optimum irradiance in the upper layers (values larger than one in Figure 2a) which states that photoinhibition is effective. During the afternoon, the effect of β is less important and photosynthesis is to a certain extent controlled by the transition zone between I_k (the light range in which photosynthesis is approximately a linear function of light) and I_{opt} (the irradiance at which photosynthesis has its maximum). In the layers below 15 m, the ambient irradiance falls below I_k , and α is the dominant photoadaptive variable.

The proportional difference between the actual photosynthesis as simulated by the model and photosynthesis as calculated from the ambient light [equations (1–3) and setting $\gamma_{\theta, \alpha, \beta, \rho_m}$ to zero, i.e. ignoring the photoadaptive process] is shown in Figure 2b. The diagram reveals that photoadaptation can affect primary production significantly. Maximum deviations can exceed 50% if photoadaptation is ignored.

This may have a consequence on the estimation of growth rates in phytoplankton in *in vitro* samples. Since the samples are in general incubated at constant depths, these measurements do not take into account the rapidly changing light environment due to turbulent mixing.

Turbulence versus static environment

In order to quantify the difference in production rates between phytoplankton moving freely in the turbulent environment and a sample held in a bottle at fixed depths, a set of non-mobile (i.e. kept at fixed depth) cells was distributed in 1 m depth intervals between the surface and 250 m (static water column). These cells follow the same rules as mobile cells, so that the difference in the photosynthetic rate is a consequence of vertical mixing only. Each morning at 05.00 h the non-mobile cells are initialized with the properties of the mobile ones. Examples of depth profiles of the photosynthetic rates in the static water column are shown in Figure 3a.

A significant difference between photosynthesis in the static water column and in the rapidly mixed one can be found (Figure 3b). The mobile cells are in general less adapted to the high subsurface irradiance than the non-mobile cells, and consequently show lower rates. Photoinhibition can occur close to the surface in the mixed-water column, but is negligible in the static one, since the light-adapted cells have a small β . Positive differences in photosynthesis occur between sunrise and noon. In the afternoon, below the near-surface layers the rapidly mixed cells tend to have higher rates than the static ones.

The depth of the euphotic layer, d (1% light level), and the daily minimum and maximum mixing layer depth at 55°N 37°W, as well as the vertically integrated

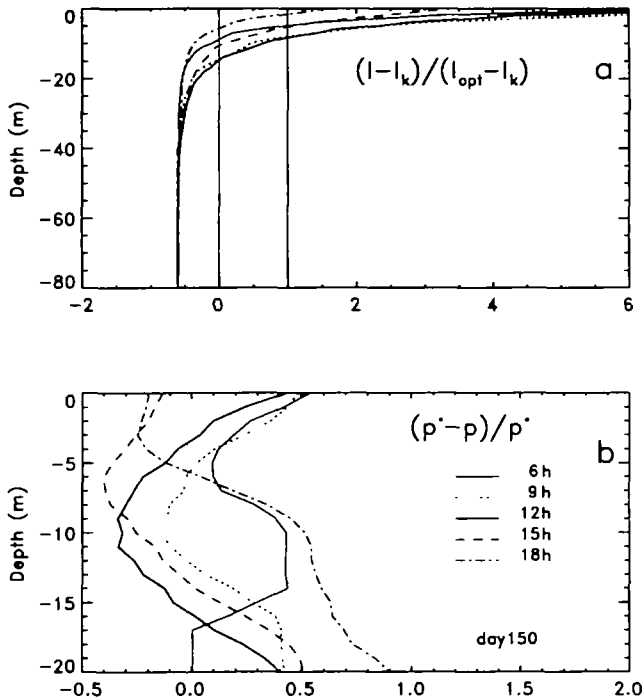


Fig. 2. (a) The ratio between $I(z) - I_k$ and $I_{opt} - I_k$ at day 150. Negative values are related to a linear relationship between photosynthesis and light, values between zero and one to a non-linear relationship, and values greater than one define the time and depth interval in which photoinhibition can become important. (b) The relative difference between the photosynthesis of fully adapted cells (p^*) and the photosynthesis calculated by the model (p).

photosynthetic rate of both the mobile (ΣC_m) and the non-mobile cells (ΣC_b) are presented in Figure 4a and b. We have chosen to compare the integrated 1 m averaged values in order to avoid any bias due to different cell concentrations in the two environments. The diagram reveals a good relationship between photosynthesis and mixing depths in both the turbulent and the static water column. The fluctuations in the static case can be explained by the daily initialization of the mobile cells. Since the cells do not adapt at night, the information of the previous afternoon is carried throughout the night, hence the non-mobile cells start each morning with a high photoadaptive state if the mixing layer was shallow and vice versa.

During the period of the bloom, the water turbidity increases, i.e. the depth of the euphotic zone is reduced, and a large amount of the solar energy is restricted to near-surface layers. The mobile cells are not able to stay sufficiently long near the surface to adapt to the higher light levels and to exploit the available energy. Consequently, the proportional difference $\delta C = (\Sigma C_b - \Sigma C_m) / \Sigma C_b$ increases with increasing water turbidity and reaches values of up to 40% towards the end of the integration, as shown in Figure 4c. The relationship between δC and the daily mixing layer minimum h_{min} suggests an overestimation of the incubation method of

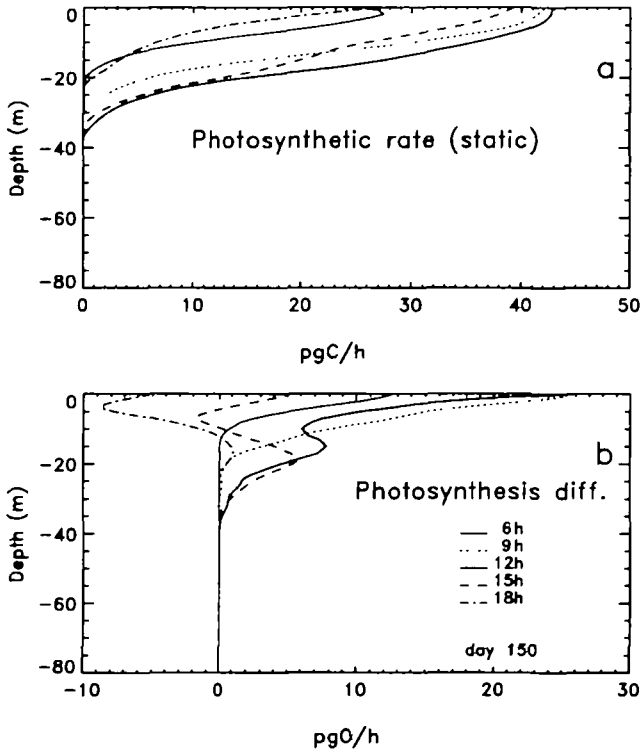


Fig. 3. (a) Profiles of photosynthesis in the static water column. (b) The deviation of the photosynthetic rate in the static water column from that in the mixed environment.

1% per 15 m mixing layer depth changes in clear water, and much higher values in turbid water (Figure 4d).

The results of a second integration carried out at 41°N 27°W are presented in Figure 5a–d. The spring bloom starts earlier in the year and its duration is shorter than that at 55°N. The decline in the photosynthetic rates in the second half of the integration is a consequence of the declining phytoplankton biomass caused by nutrient limitation and increased grazing. In this period, the differences are reduced and can even become negative, whilst during the spring bloom, primary production in the turbulent water column is always smaller than in the static one. The proportional difference δC on average shows an increase towards the second half of the spring bloom with values between 20 and 30% (Figure 5c).

A method to correct *in vitro* incubation measurements

The results presented in Figure 4d are divided into three stages according to the optical properties that the model water column experiences during the spring bloom (Figure 6), which are: (i) the clear-water case of the first 40 days of the integration period (low phytoplankton abundance); (ii) a transition zone in which the base of the euphotic zone rises from deeper layers towards the near surface region; and (iii) the turbid water period during the remaining 50 days of the bloom (high phytoplankton abundance).

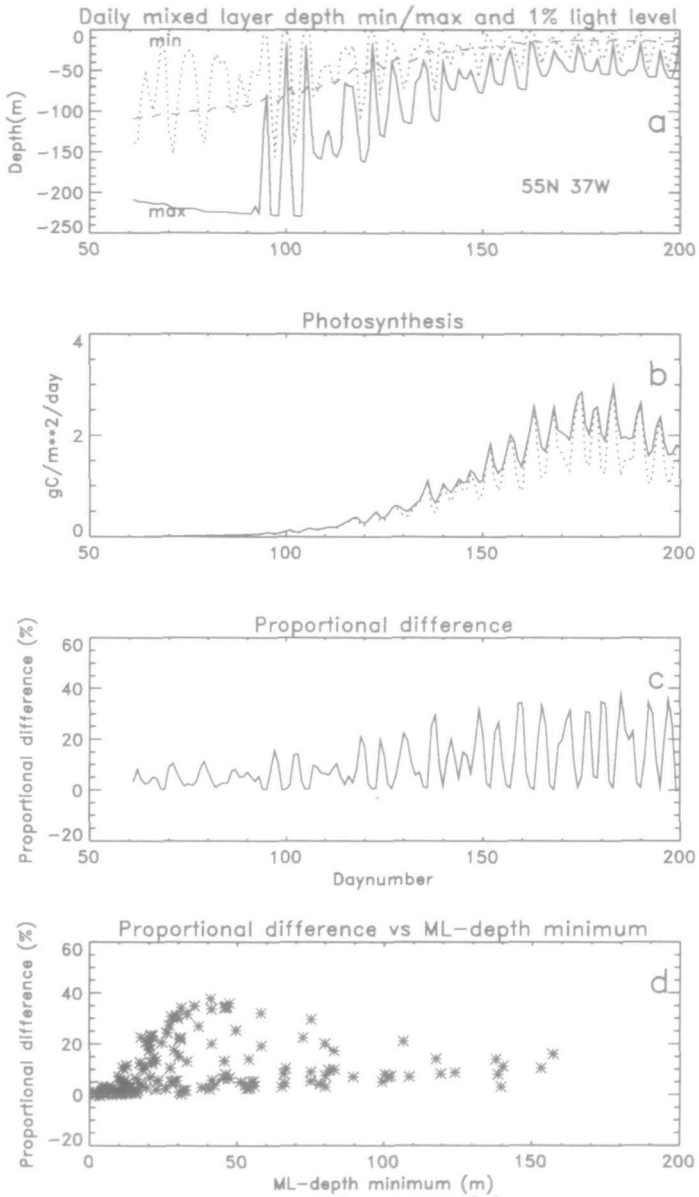


Fig. 4. (a) Daily minimum and maximum of the depth of the mixing layer and the depth of the euphotic layer (1% light level) at 55°N 37°W. (b) The vertically integrated daily photosynthetic rates in both the static and in the mixed environment. Continuous line: static; dashed line: mixed. (c) Proportional difference between photosynthetic rates in the static and in the mixed-water column. (d) Proportional difference versus daily mixing layer depth minimum.

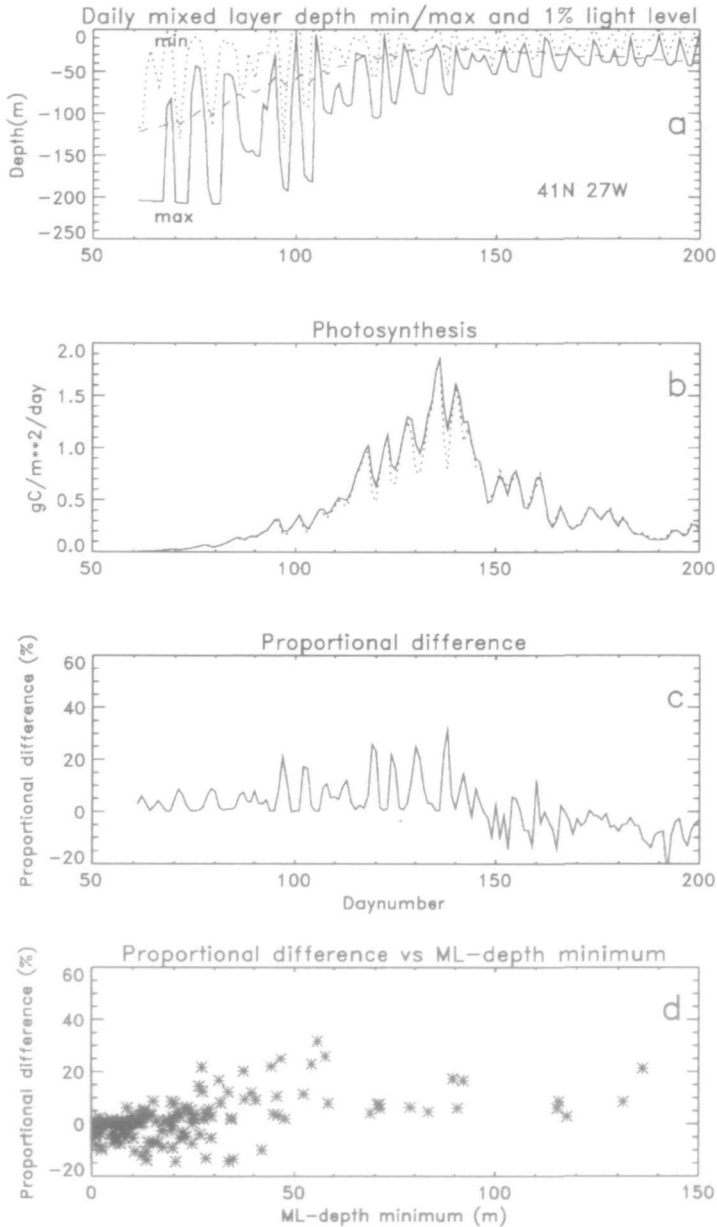


Fig. 5. As in Figure 4, but for 41°N 27°W.

Stages (i) and (iii) are characterized by almost constant depths of the euphotic layer and by nearly linear relationships between δC and h_{min} with values of 0.07 and 1% m^{-1} , respectively, whilst in stage (ii) the values of δC range from 0.07 to 0.6% m^{-1} .

The results so far indicate that not only the mixing depths, but also the water turbidity, play an important role for photoadaptive and photosynthetic processes

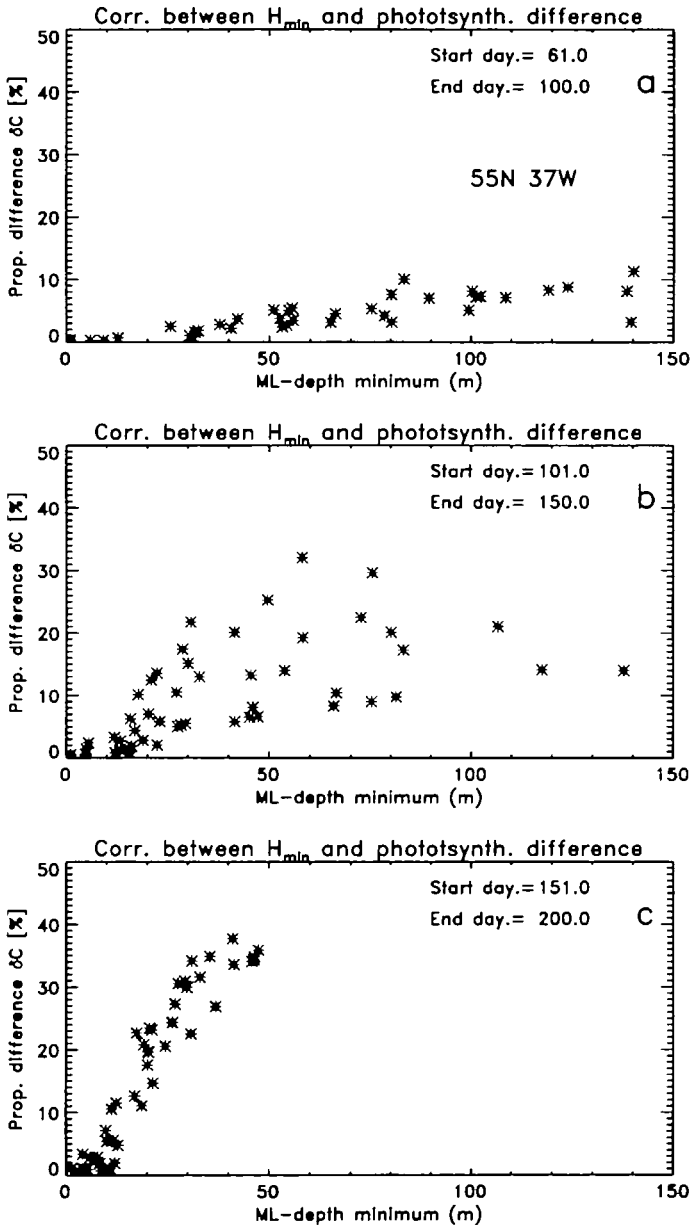


Fig. 6. Relationship between the proportional difference and the daily mixing layer depth minimum, h_{min} , for three different time periods.

in the turbulence environment of the upper ocean boundary layer. A similar conclusion can be drawn from the Lande and Lewis (1989) bulk model, in which the difference between photoadaptive parameters in a static and a mixed environment also depends on the attenuation coefficient for scalar irradiance.

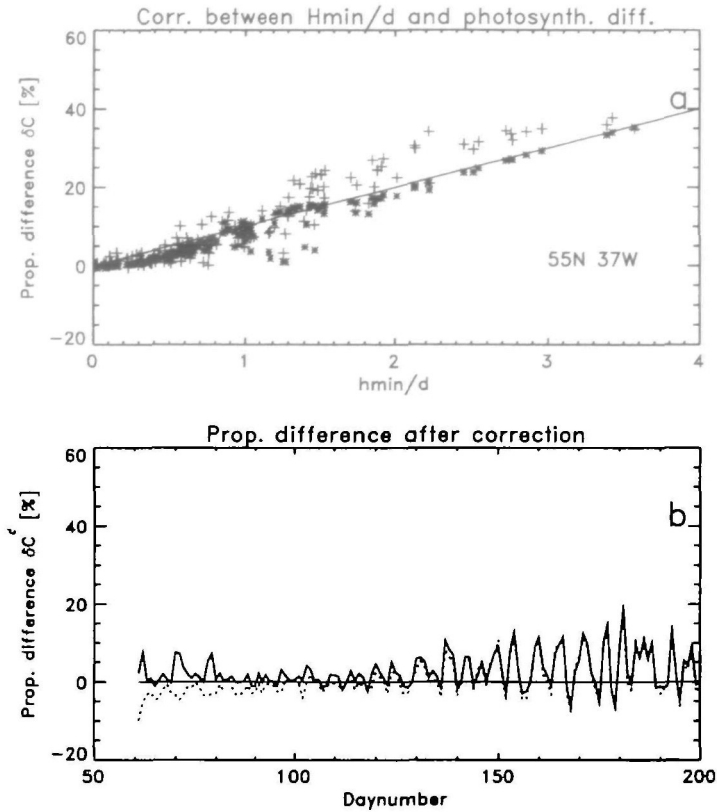


Fig. 7. (a) Relationship between the proportional difference (+++) and the ratio h_{min}/d , and the calibration function Y (***) at 55°N 37°W. (b) Proportional differences after correction (dashed line: linear correction; continuous line: non-linear correction).

In order to correct *in vitro* incubation measurements of primary production for turbulence, both water turbidity and mixing depths have to be taken into account. Assuming a linear relationship between δC and h_{min}/d (Figure 7a), the corrected photosynthetic rate ΣC_b^c may simply be expressed as a function of the measured photosynthetic rate ΣC_b , the mixed layer depth h_{min} and the depth of the euphotic zone, d :

$$\Sigma C_b^c = \Sigma C_b(1 - Kh_{min}/d)$$

where $K = 10\%$ is a proportionality constant that depends on the phytoplankton specifications. The corrected values for $(\Sigma C_b^c - \Sigma C_m)/\Sigma C_m$ are presented in Figure 7b.

The linear correction term is capable of reducing δC , but it has two disadvantages: (i) the approximation is empirical and (ii) there is a shift of δC towards mainly negative values during the start of the bloom, implying an underestimation of the corrected *in vitro* measurements for smaller h_{min} .

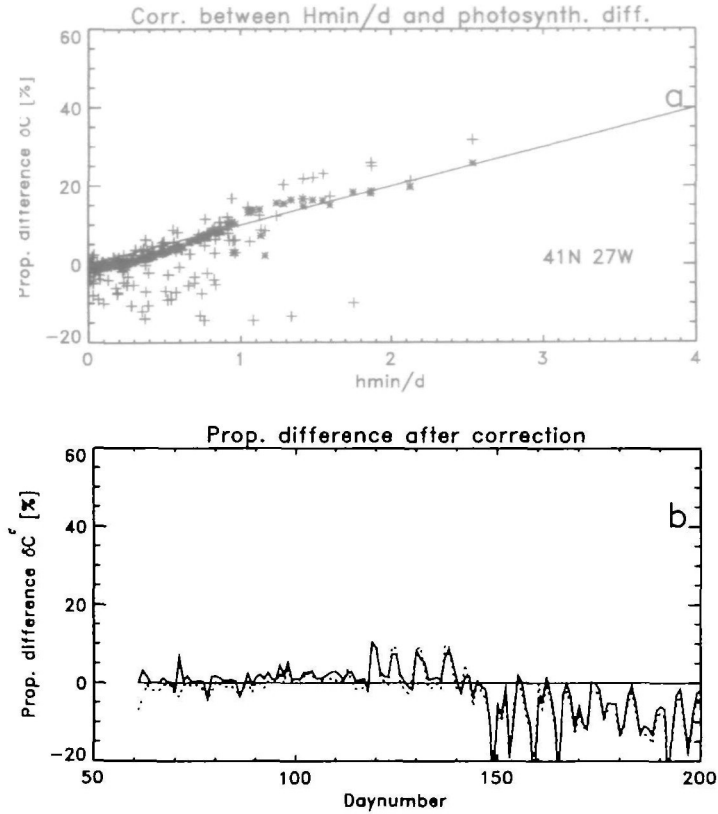


Fig. 8. As in Figure 7, but for 41°N 27°W.

In order to consider the photoadaptive parameters explicitly and to improve the correction, two simple models were constructed from equation (1).

In the static environment:

$$P^s = \theta^s P_m^s \left(1 - e^{-\frac{\alpha^s I}{P_m^s}} \right) e^{-\frac{\beta^s I}{P_m^s}} \quad (5)$$

in which P^s presents the photosynthetic rate, and the photoadaptive variables X_i^s (α , β , θ , P_m) are defined according to equation (2):

$$X_i^s = b_i + a_i \ln(I), \quad (i = 1, 4) \quad (5a)$$

In the turbulence environment:

$$P^t = \theta^t P_m^t \left(1 - e^{-\frac{\alpha^t I}{P_m^t}} \right) e^{-\frac{\beta^t I}{P_m^t}} \quad (6)$$

The photoadaptive variables are derived from equation (5a) by assuming X_i^t to be constant in the mixing layer and by varying X_i^t linearly with depth. Thus

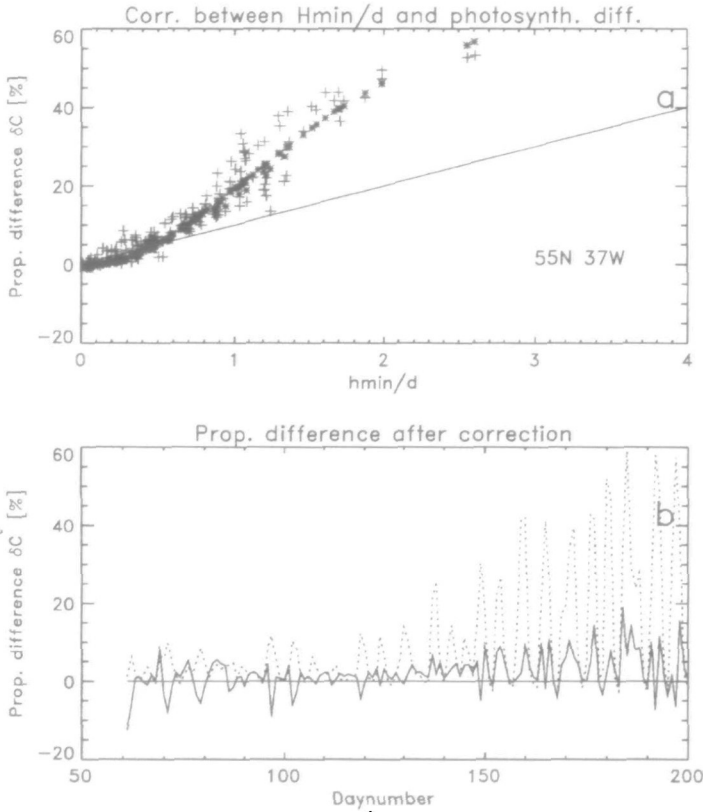


Fig. 9. (a) Relationship between the proportional difference (+++) and the ratio h_{min}/d , and the calibration function Y (***) at 55°N 37°W. Photosynthesis was calculated by means of a constant carbon-chlorophyll ratio. (b) Proportional differences after correction (dashed line: linear correction; continuous line: non-linear correction).

$$X_i^* = [X_i^*(0) + X_i^*(h_{min})]/2 \quad \text{for } h_{min} \leq z_i^*$$

and

$$X_i^* = X_i^*(z_i^*) + \frac{z_i^*}{2h_{min}} [X_i^*(0) - X_i^*(z_i^*)] \quad \text{for } h_{min} > z_i^*$$

where z_i^* equal the depths at which X_i^* remain constant. In this study, we chose the values 12.5, 0.0, 0.05 and 0.003 for θ , P_m , α and β , respectively.

To simplify the two equations further, the irradiance profile is approximated by $I(z) = I_0 e^{-\kappa z}$, where the attenuation coefficient κ is related to the depth of the euphotic zone ($\kappa = \ln(100)/d$).

Using h_{min} and d from Figure 4a, and the daily average surface irradiance I_0 , equations (5) and (6) are numerically integrated over the entire water column and the proportional differences $(\sum P^* - \sum C^*)/\sum P^* = Y$ are calculated for each day. The non-linear function $Y=f(h_{min}/d)$, as presented in Figure 7a, reduces δC by ~50% (Figure 7b), and occasional negative values are small ($\sum C_b^* = \sum C_b (1 - Y)$).

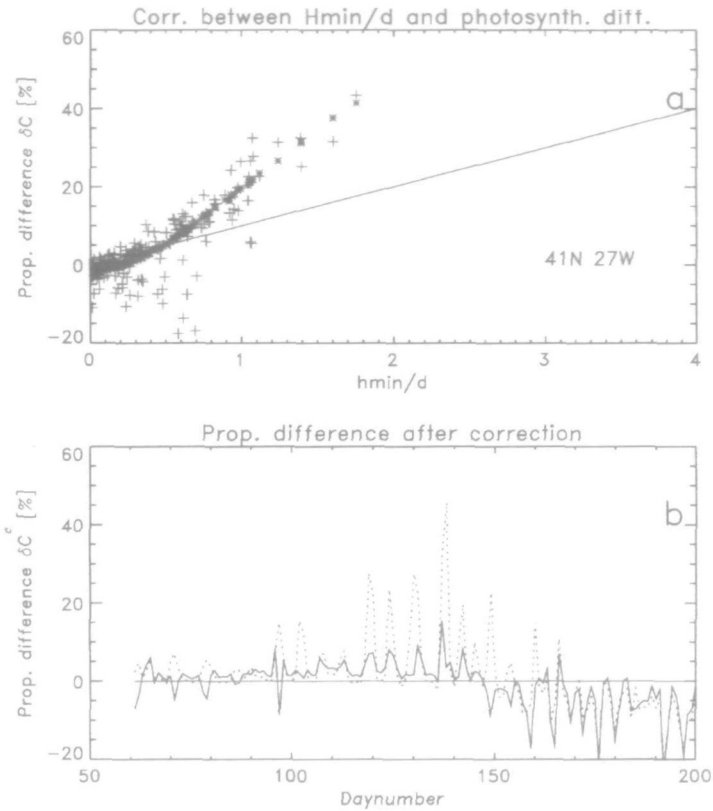


Fig. 10. As in Figure 9, but for 41°N 27°W.

So far, the corrections were discussed for an integration carried out at 55°N 37°W. The same method was applied at a location off the Azores. Here, reductions of 50% can be achieved, and in general unrealistic negative values can be avoided during the spring bloom (Figure 8). The method cannot be applied when primary production becomes nutrient limited.

The relationships between δC and h_{\min}/d are close to being linear. Additional experiments were carried out in which the carbon–chlorophyll ratio was kept constant. The dependencies were found to be highly non-linear and consequently a linear correction cannot be applied any more. Our simple model [equations (5) and (6)] achieves more reliable corrections than a linear function (Figures 9 and 10) and may be suitable to reduce overestimations for a variety of plankton populations.

Summary and discussion

A modified version of the Woods and Barkmann (1994) Lagrangian Ensemble model was used to study the behaviour of photoadaptive properties of the diatom *T.pseudonana* in a static environment, representing *in vitro* incubation measurements of primary production in the upper ocean, and in a turbulence environment.

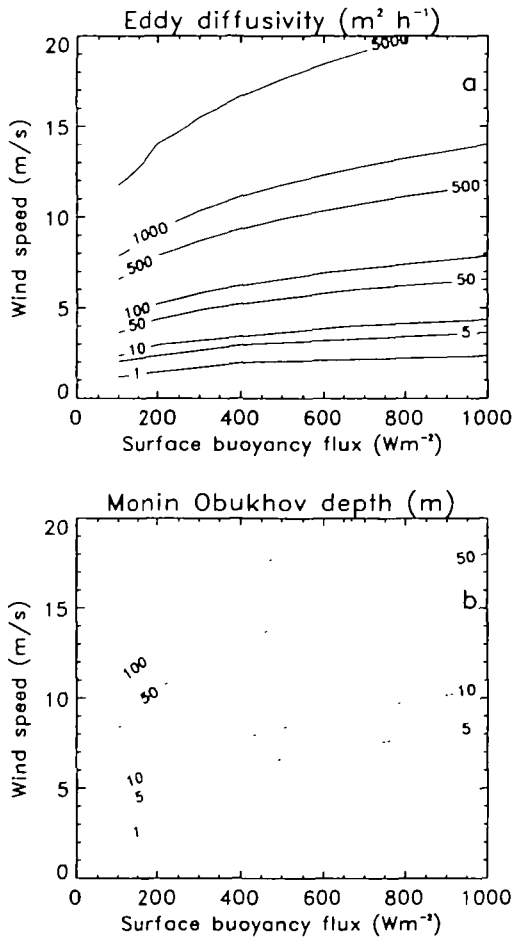


Fig. 11. (a) Eddy diffusion coefficient as a function of wind speed and surface buoyancy flux. (b) Monin-Obukhov depth as a function of wind speed and surface buoyancy flux.

In this study, primary production of non-mobile diatoms (static) is in general higher than that of plankton cells moving freely in the turbulent boundary layer. The simulation model predicts differences in the vertically integrated photosynthetic rates of up to 40%, caused by the mixing effect of turbulence on the photo-adaptive properties of the diatom. These differences are higher than those predicted by Lande and Lewis (1989) and Falkowski and Wirick (1981). The discrepancy between the numerical studies can be explained by the different mixing time scales used in the studies.

Following the arguments of Denman and Gargett (1983), the Lagrangian rms vertical displacements (Z_m) of a particle in a well-mixed layer can be expressed by $Z_m^2 = 2u_*^2 T_L t$, where the Lagrangian time scale T_L can be approximated by the Eulerian one, i.e. $T_L \sim 1/3T_E = L_v/(3u_*)$, and the turbulent velocity u_* equals twice the friction velocity u_* . On the other hand, when stratification becomes important,

$u^2 T_L$ may be replaced by a vertical turbulent diffusion coefficient k_v , so that $Z_m^2 = 2k_v t$. To clarify the difference between the two approaches, we assume that Z_m equals Z , and calculate the corresponding diffusion coefficient from $k_v = u \cdot L_b / 2/3$, where L_b is a buoyancy length scale.

In a diurnally varying mixing layer, the only buoyancy source during the daytime which can create stratification is the net surface buoyancy flux (neglecting a possible vertical buoyancy flux caused by horizontal buoyancy advection and vertical current shear; Rodhe, 1991), and the appropriate buoyancy length scale of the energy-containing eddies should then be the Monin–Obukhov depth, $L_{MO} = L_b = u^2 / (\kappa B)$ ($\kappa = 0.4$ is von Karman's constant and B is the net surface buoyancy flux). In this case, the diffusion coefficient k_v is a function of the wind stress and the buoyancy flux ($k_v = 2u^2 / (3\kappa B)$). L_{MO} and k_v as functions of various surface fluxes and wind speeds are displayed in Figure 11a and b. It is immediately apparent that eddy diffusivities of $40 \text{ m}^2 \text{ h}^{-1}$ as used by Lande and Lewis (1989) or $3.6 \text{ m}^2 \text{ h}^{-1}$ (Falkowski and Wirick, 1981) are not capable of creating vertical eddy length scales $> 5 \text{ m}$. For example, in a 20 m deep surface layer, the mixing time scales are of order 10 and 100 h, respectively. Our approach, using $u^2 T_L$ rather than a small k_v to calculate particle displacements, reveals mixing time scales of order 1 h which are smaller than the adaptation time scales of the photoadaptive variables, and consequently predicts significant differences in photosynthesis between bottles held at a fixed depth and plankton cells moving freely in the turbulence environment from mixing depths $> 20 \text{ m}$.

By simplifying the photoadaptive parameters in the PI relationship, and assuming that the time scale for mixing is always smaller than the adaptation time scale, a calibration function was calculated relating deviations in photosynthetic rates of non-mobile diatoms from those of mobile cells to the three environmental variables: surface irradiance, minimum depth of the daily mixing layer and water turbidity. This non-linear function was applied to calibrate the simulated *in vitro* incubation measurements. The results indicate that overestimations could be reduced by 40–50%. After correction, typical maximum differences of 15% can be found. However, the calibration function is not able to explain the mainly positive deviations from the existing non-linear trend (Figures 7a, 8a, 9a and 10a). A possible cause for these fluctuations may be the effect the diurnal cycles of mixing and surface irradiance have on the statistical properties of the mobile plankton population (Woods and Onken, 1982).

We conclude from our model results that *in vitro* incubation measurements in upper ocean boundary layers have the tendency or at least the potential to overestimate the productivity of phytoplankton populations with photoadaptive properties similar to the ones we have studied. The degree of this overestimation depends to the first approximation on the water turbidity (acting as a magnifying factor), on the mixing depth, and on the relationship between the time scales of photoadaptation and vertical mixing.

Changes in spectral light quality may contribute to further uncertainties in the incubation measurements. Phytoplankton in general respond physiologically to changes in the spectral distribution of light (e.g. Rivkin, 1989; Nielsen and Sakshaug, 1993). For example, the photosynthetic efficiency, α , of the diatom

T.pseudonana appears to be relatively high if adapted to blue light and low if grown in a green-light regime (Glover *et al.*, 1987). Taking the spectral dependency of the photoadaptive variables into account, the effective depth of the euphotic zone may be smaller than predicted by the model, and the difference in photosynthesis between mobile and non-mobile cells could be higher than estimated in this study.

In vitro measurements in coastal areas or in continental shelf regions with strong tidal flows, where the water is in general more turbid than in the open ocean and tidal currents can force the bottom boundary layer to merge with the upper mixed layer, thereby causing a deep turbulent layer even in moderate wind conditions, may have the tendency to produce overestimated values even higher than those in the open ocean.

Enhanced mixing may occur at the continental shelf edge, where tidally generated internal waves can develop into high-frequency (~1 h period) internal solitary waves with amplitudes of order 20–50 m and wavelength of order 100 m (Sandström and Oaky, 1995). The associated turbulent layers caused by the current shear instability are observed to be periodic and confined to a 10–15 m thick layer near the maximum density gradient (Sandström *et al.*, 1989). The internal wave motion, as well as vertical mixing due to breaking internal waves, may create a favourable environment for phytoplankton growth, but has not been taken into account in the present study.

In this study, we applied photoadaptive properties of the diatom *T.pseudonana* for the comparison in mixed and static conditions; the numerical model is however able to carry out a comparison for any oceanic phytoplankton population on condition that the relationships between photoadaptive parameters and changing light are known.

References

- Byshev, V.I., Ivanov, Yu.A. (1969) The time spectra of some characteristics of the atmosphere above the ocean. *Izvestia. Atmos. Ocean Phys.* **5**, 17–28
- Cullen, J.J. and Lewis, M.R. (1988) The kinetics of algal photoadaptation in the context of vertical mixing. *J. Plankton Res.*, **10**, 1039–1063.
- De Baas, A.F., van Dop, H. and Nieuwstadt, F.T.M. (1986) An application of the Langevin equation for inhomogeneous conditions to dispersion in a convective boundary layer. *Q. J. R. Meteorol. Soc.*, **112**, 163–180.
- Denman, K.L. and Gargett, A.E. (1983) Time and space scales of vertical mixing and advection of phytoplankton in the upper ocean. *Limnol. Oceanogr.*, **28**, 801–815.
- Falkowski, P.G. and Wirrick, C.D. (1981) A simulation model of the effects of vertical mixing on primary productivity. *Mar. Biol.*, **65**, 69–75.
- Gallegos, G.L. and Platt, T. (1982) Plankton production and water motion in surface mixed layers. *Deep-Sea Res.*, **29**, 65–76.
- Glover, H.E., Keller, M.D. and Spinrad, R.W. (1987) The effects of light quality and intensity on photosynthesis and growth of marine eukaryotic and prokaryotic phytoplankton clones. *J. Exp. Mar. Biol. Ecol.*, **105**, 137–159.
- Hall, C.D. (1975) The simulation of particle motion in the atmosphere by a numerical random walk model. *Q. J. R. Meteorol. Soc.*, **101**, 235–244.
- Horch, A., Barkmann, W. and Woods, J.D. (1983) *Die Erwärmung des Ozeans hervorgerufen durch solare Strahlungsenergie*. Berichte aus dem Institut fuer Meereskunde, Nr. 120, 190 pp.
- Isemer, H.-J. and Hasse, L. (1986) *The Bunker Climate-Atlas of the North Atlantic Ocean*. Springer Verlag, Berlin.
- Kraus, E.B. and Turner, J.S. (1967) A one-dimensional model of the seasonal thermocline. II. The general theory and its consequences. *Tellus*, **13**, 231–238.

- Lande, R. and Lewis, M.R. (1989) Models of photoadaptation and photosynthesis by algal cells in a turbulent mixed layer. *Deep-Sea Res.*, **36**, 1161–1175.
- Lewis, M.R., Cullen, J.J. and Platt, T. (1984) Relationships between vertical mixing and photoadaptation: similarity criteria. *Mar. Ecol. Prog. Ser.*, **15**, 141–149.
- Marra, J. (1978a) Effect of short-term variations in light intensity of photosynthesis of a marine phytoplankton: a laboratory simulation study. *Mar. Biol.*, **46**, 191–203.
- Marra, J. (1978b) Phytoplankton photosynthesis response to vertical movement in the mixed layer. *Mar. Biol.*, **46**, 203–208.
- Morel, A. (1988) Optical modelling of the upper ocean in relation to its biogenous matter content (case I waters). *J. Geophys. Res.*, **93**, C9, 10749–10768.
- Nielsen, M.V. and Sakshaug, E. (1993) Photobiological studies of *Skeletonema costatum* adapted to spectrally different light regimes. *Limnol. Oceanogr.*, **38**, 1576–1581.
- Paltridge, G.W. and Platt, C.M.R. (1976) *Radiative Processes in Meteorology and Climatology*. Elsevier, Amsterdam.
- Platt, T., Gallegos, C.L. and Harrison, W.G. (1980) Photoinhibition of photosynthesis in natural assemblages of marine phytoplankton. *J. Mar. Res.*, **38**, 687–701.
- Rivkin, R.B. (1989) Influence of irradiance and spectral quality on the carbon metabolism of phytoplankton. I. Photosynthesis, chemical composition and growth. *Mar. Ecol. Prog. Ser.*, **55**, 291–304.
- Rodhe, J. (1991) Wind mixing in a turbulent surface layer in the presence of a horizontal density gradient. *J. Phys. Oceanogr.*, **21**, 1080–1083.
- Sandström, H. and Oakey, N.S. (1995) Dissipation in internal tides and solitary waves. *J. Phys. Oceanogr.*, **25**, 604–614.
- Sandström, H., Elliot, J.A. and Cochrane, N.A. (1989) Observing groups of solitary waves and turbulence with Batfish and Echo-Sounder. *J. Phys. Oceanogr.*, **19**, 987–997.
- Steele, J.H. (1962) Environmental control of photosynthesis in the sea. *Limnol. Oceanogr.*, **7**, 137–150.
- Tennekes, H. and Lumley, J.L. (1972) *A First Course in Turbulence*. Massachusetts Institute of Technology, The MIT Press, 300 pp.
- Thomson, D.J. (1986) A random walk model of dispersion in turbulent flows and its application to dispersion in a valley. *Q. J. R. Meteorol. Soc.*, **112**, 511–530.
- Woods, J.D. (1968) Wave-induced shear instability in the summer thermocline. *J. Fluid Mech.*, **32**, 791–800.
- Woods, J.D. (1980) Diurnal and seasonal variation of convection in the wind mixed layer of the ocean. *Q. J. R. Meteorol. Soc.*, **106**, 379–394.
- Woods, J.D. and Barkmann, W. (1986) The response of the upper ocean to solar heating. I: The mixed layer. *Q. J. R. Meteorol. Soc.*, **112**, 1–27.
- Woods, J.D. and Barkmann, W. (1993) The plankton multiplier-positive feedback in the greenhouse. *J. Plankton Res.*, **15**, 1053–1074.
- Woods, J.D. and Barkmann, W. (1994) Simulating plankton ecosystems by the Lagrangian Ensemble method. *Phil. Trans. R. Soc. London Ser. B*, **343**, 27–31.
- Woods, J.D. and Onken, R. (1982) Diurnal variation and primary production in the ocean—preliminary results of a Lagrangian Ensemble method. *J. Plankton Res.*, **4**, 735–756.
- Yamazaki, H. and Kamykowski, D. (1991) The vertical trajectories of motile phytoplankton in a wind-mixed water column. *Deep-Sea Res.*, **38**, 219–241.
- Yoder, J.A. and Bishop, S.S. (1985) Effects of mixing-induced irradiance fluctuations on photosynthesis of natural assemblages of coastal phytoplankton. *Mar. Biol.*, **90**, 87–93.

Received on June 28, 1995; accepted on December 22, 1995

Appendix: Table of symbols and definitions

Photosynthesis and nutrient uptake

C	carbon content of a plankton cell
R_p	CO ₂ loss due to respiration
θ	carbon–chlorophyll ratio
α	initial slope of the PI curve
P_m	photosynthesis at light saturation
β	photoinhibition parameter
$\gamma_{\alpha, \beta, P_m, \theta}^{-1}$	time scales of photoadaptation
$b_{\alpha, \beta, P_m, \theta}$	cell-specific constants
$a_{\alpha, \beta, P_m, \theta}$	cell-specific constants
$I(z)$	light level at depth z (400–700 nm)
I_k	P_m/α
I_{opt}	light at maximum photosynthesis
N	nitrate concentration
A	ammonium concentration
k_N, k_A	half-saturation constants
N_p	nitrogen content of a plankton cell

Particle motion in a turbulent boundary layer

V	particle velocity
τ	Lagrangian time scale
$d\xi$	random velocity increment
$\overline{u^2}$	velocity variance in turbulent layer
dt	time increment
h	depth of turbulent layer
ϵ_m	dissipation rate
λ	e-folding depth
l_e	dissipation length scale
TKE	turbulent kinetic energy
P_c	TKE source generated by convection
m, n	model parameters

Results section

ΣC_m	vertically integrated photosynthetic rate of mobile cells
ΣC_b	vertically integrated photosynthetic rate of non-mobile cells
δC	proportional difference between photosynthetic rates
h_{mix}	daily minimum mixed-layer depth

Method to correct in vitro incubation measurements

d	depth of the euphotic zone
ΣC_b^c	corrected photosynthetic rate
K	proportionality coefficient
X_s^p	photosynthetic variables θ, α, β and P_m in the static water column
X_t^p	photosynthetic variables θ, α, β and P_m in the turbulent water column
P^s	photosynthetic rate in the static water column
P^t	photosynthetic rate in the turbulent water column
κ	light attenuation coefficient
$\overline{I_0}$	daily averaged surface irradiance
Y	calibration function